

Mode-Locked Diode Laser for Precision Optical Frequency Measurements

A final report submitted in partial fulfillment of requirements
for the degree of Bachelor of Science in Physics
from the College of William and Mary in Virginia.

Trevor Harrison

Advisor: Seth Aubin

Research Coordinator: Gina Hoatson

Williamsburg, Virginia

May 2009

Abstract:

This thesis presents an actively mode-locked diode laser as the source of an optical frequency comb with a bandwidth of at least 200 GHz. A mode-locked laser is composed of a broadband spectrum of discrete frequencies – a comb – that interferes, generating a pulsed laser output. The spectral width of the comb is inversely proportional to the temporal pulse width. In this research, an external cavity is introduced to a diode laser, and the laser's gain medium is directly modulated using an RF signal. Using a Michelson interferometer for autocorrelation measurements, pulses as short as 10 ps have been observed. A scanning Fabry-Perot interferometer was constructed to directly observe the comb, but implementation has not been successful due to alignment difficulties. It is believed that pulses as short as 1 ps could eventually be generated, corresponding to a comb width of between 318 THz and 1 THz. When completed, the optical frequency comb will be used to make precision optical frequency measurements in the Ultra-cold Atomic, Molecular and Optical physics laboratory.

Acknowledgements

With the sincerest gratitude I can offer, I would like to thank the following people: Dr. Seth Aubin – for your time, energy, patience, and guidance; Dr. Gina Hoatson – for the time and energy spent overseeing all of the senior research; Dr. Jan Chaloupka – for your advice and optics components; Brian DeSalvo – for building the laser and initiating the research; friends and family – for everything.

Thanks.

Table of Contents:	Page:
1. Introduction	6
2. Theory	8
2.1 Optical Frequency Comb	8
2.3 Mode-Locked Lasers	9
2.4 Mode-Locking Methods	10
3. Laser Apparatus	12
3.1 Laser Diode Operating Modes	14
3.2 Preliminary Pulse Analysis with Fast Photodiode	14
4. Sub-Nanosecond Pulse Detection Methods	17
4.1 Scanning Fabry-Perot Cavity	17
4.2 Michelson Interferometer as Autocorrelator	18
4.2.1 First Order Autocorrelation – Theory	20
4.2.2 Second Order Autocorrelation – Theory	21
5. Detection of Picosecond Pulses	22
5.1 Experimental Implementation of Michelson Interferometer	22
5.1.1 First Order Autocorrelation – Results	23
5.1.2 Second Order Autocorrelation – Results	25
6. Conclusion	30
References	32
Appendix A: Standard Operating Procedure	33

List of Images and Tables:	Page:
Fig 1: Frequency Stabilization by Application of Optical Frequency	7
Fig. 2: Multi-mode output of laser	8
Fig. 3: Output of laser in Frequency space.	9
Fig. 4a and 4b: Simplified Output of Multi-mode laser	10
Fig. 5: Schematic diagram of active mode-locking diode laser	12
Fig. 6: Laser Diode and External Cavity	13
Fig. 7: Nanosecond Pulses, as measured by Fast Photodiode	14
Fig. 8: Frequency vs. Pulse Magnitude (RMS)	15
Fig. 9: Gain Modulation Frequency v. Pulse Temporal Full-Width	16
Fig. 10: Custom Fabry-Perot	18
Fig. 11: Michelson Interferometer as Autocorrelator	19
Table 1: Translation Stage Change Δx for Temporal Overlap $\Delta \tau$	22
Fig. 12: Experimental Setup of Michelson Interferometer as Autocorrelator	23
Fig. 13: Fringe Visibility	24
Fig. 14: Blue Light vs. Red Light Attenuation	26
Fig. 15: Second Order Autocorrelation	28
Fig. 16: Second Order Autocorrelation – Attenuated Light	39
Fig. 17: Second Order Autocorrelation for “Continuous Wave” Laser Output	30

1. Introduction

Precision optical frequency measurements are difficult due to their very high frequencies in the range of 15 – 1500 THz [1] and there currently exist no electronic methods for directly measuring frequencies in this range [4]. Theodor W. Hänsch and John L. Hall developed the optical frequency comb as a solution to this problem, work for which they were awarded half of the 2005 Nobel Prize in Physics. This research project is motivated by the need to lock, or stabilize, a laser at a particular frequency, defined by energy transitions for ultra-cold KRb molecule generation or alternatively in ultra-cold francium atom generation, though the method should be widely applicable to other systems as well. While normal electronic methods for frequency measurement and stabilization do not work for such exotic spectroscopic systems, optical frequency combs offer a solution.

Stabilization via an optical frequency comb (OFC) begins with one extremely stable laser with an output at the frequency, ω_0 , of well known atomic transition, as shown in Figure 1. A second laser provides the comb of discrete frequencies pictured in blue in Figure 1. The third laser, with frequency ω_1 , requires stabilization. First, the OFC is locked to the atomically stable laser by electronically stabilizing the difference $\Delta\omega_0$ between ω_0 and the closest comb frequency. Shining the stabilized OFC onto a detector along with the laser to be stabilized produces a beat frequency equal to the difference $\Delta\omega_1$ between the laser and the nearest comb tooth. Electronically stabilizing this difference thus transfers the extremely precise nature of the atomic transition to the laser. Counting the number of comb teeth between the atomic transition laser and the stabilized laser offers a precise frequency measurement.

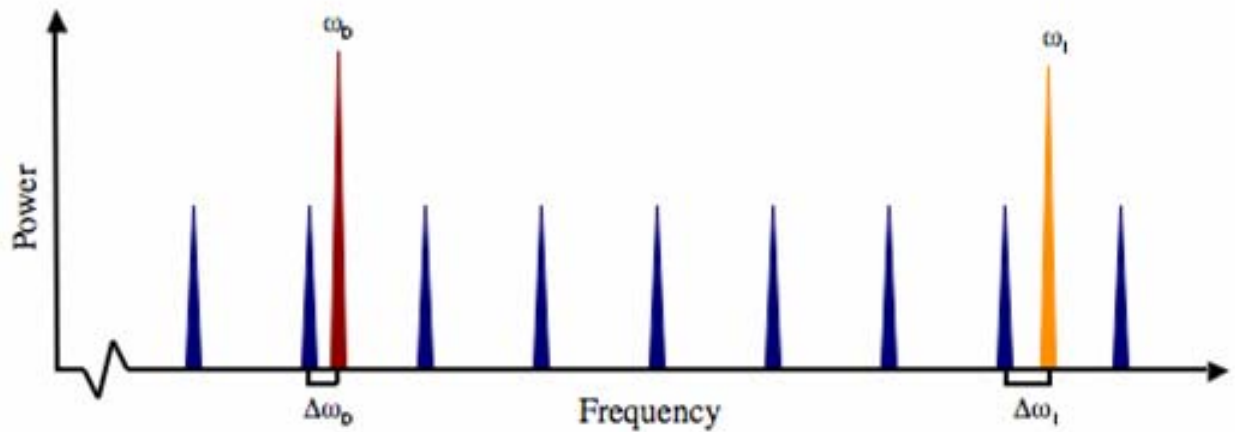


Fig. 1: Frequency Stabilization by Application of Optical Frequency Comb An optical frequency comb, outputting a discrete spectrum of evenly spaced frequencies, indicated in blue, is electronically locked at frequency $\Delta\omega_0$ to a laser with frequency ω_0 based on an atomic transition. A laser in need of stabilization, frequency ω_1 , is then electronically locked with frequency difference $\Delta\omega_1$ to the optical frequency comb. This method allows precise optical frequency measurements in the THz range.

While they are becoming commercially available, typical optical frequencies combs are based on Titanium Sapphire lasers and are prohibitively expensive, costing around \$275,000. Though Ti:Sapph OFCs do offer comb widths of upwards of 100 THz, careful consideration of experimental needs indicates such widths may be unnecessary. Consider the laser trapping of francium as an example: the wavelength needed is 718.216 nm in vacuum. Produced by Neon I, the nearest viable transition line for use in stabilization has a wavelength of 717.394 nm. The wavelength difference of .882 nm will require an optical frequency comb about 1 THz in spectral width for stabilization. Considering the cost, a 100 THz comb becomes excessive, and in response, this research attempts to produce 1 THz comb using a diode laser set-up, substantially decreasing the cost, without affecting performance.

2 Theory

2.1 Optical Frequency Comb

Optical frequency combs are a broadband set of evenly spaced, discrete frequencies and are an example of multi-mode output from lasers. OFCs begin with a multi-mode laser, continuously emitting in as many different modes, or frequencies, as the lasing gain medium can support. The electromagnetic laser fields of the optical frequency comb interfere in time, creating a pulsed output, as observed in Fig 2. Performing a Fourier transform of the pulse gives the laser output in frequency space, shown in Figure 3. From this depiction of frequency space, the analogy of OFCs as a ruler in frequency space becomes clear.

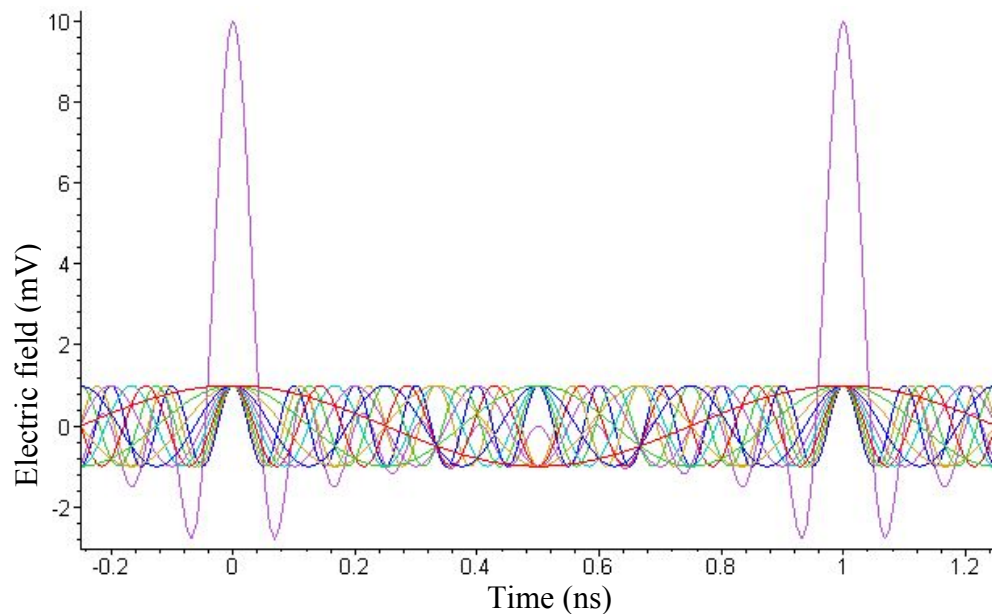


Fig. 2: Multi-mode output of laser. All the frequencies interfere in time, producing a pulsed output. As the laser produces more frequencies, the pulses become shorter. The output between pulses also goes to zero due to destructive interference.

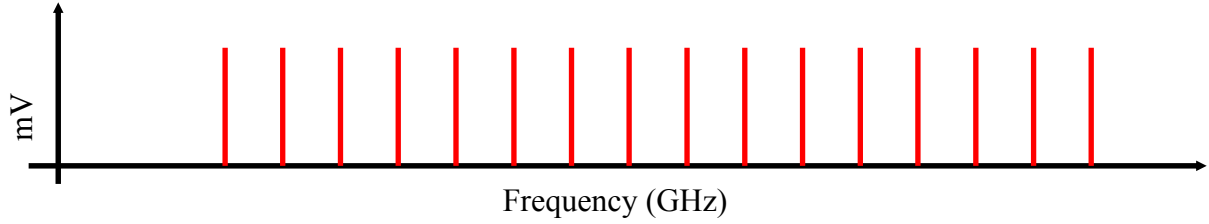


Fig. 3: Output of laser in Frequency space. This is a Fourier transform of Fig. 2. We observe the broad spectrum of discretely spaced frequencies forming the comb. With a multi-mode laser, a comb tooth's amplitude depends on how much of the gain bandwidth is amplifying a particular frequency. In the above model, all modes were given equal weight. Ideally, each sine wave form a Dirac delta function in frequency space.

The relationship between the temporal width of the pulses and the spectral bandwidth of the laser is expressed by the transform equation:

$$\Delta \omega \Delta t \geq 1 \quad (1)$$

where $\Delta \omega$ is the spectral width of the gain medium, and Δt is the full temporal width of the pulses at half the max intensity [3]. Therefore, minimizing pulse width will tend to maximize comb width. The resolution of the comb, the spacing between each comb tooth, is equal to the pulse repetition rate, typically in the 100 MHz to 10 GHz range.

2.2 Mode-Locked Lasers

For multi-mode lasers, mode-locked lasers produce the shortest pulses. Mode-locking is the condition where the phase difference between the multiple outputted frequencies have a linear relation or are all constant. In order to better understand mode locked output and deviations from it, a numerical model was created based on the following equations. The starting electric field description for a comb with 21 teeth:

$$E = \sum_{j=-10}^{10} E_j e^{i(\omega_0 + j\Delta\omega_{cavity})t + i\phi_j} \quad (2)$$

where E_j is the amplitude of each mode and was left constant, ω_0 is the central optical frequency of the laser, and $\Delta\omega_{\text{cavity}}$ is the mode spacing, determined by the geometry of the set-up.

A comparison of pulse outputs for different phase relations is shown in Fig. 4a and Fig. 4b. Figure 4a depicts the laser output when there is a square phase relation between modes ($\phi_j = \phi_0 j^2$). Figure 4b depicts the laser output when the phases are all equal ($\phi_j = \phi_0$). This example illustrates that mode-locking produces the shortest and most intense pulses.

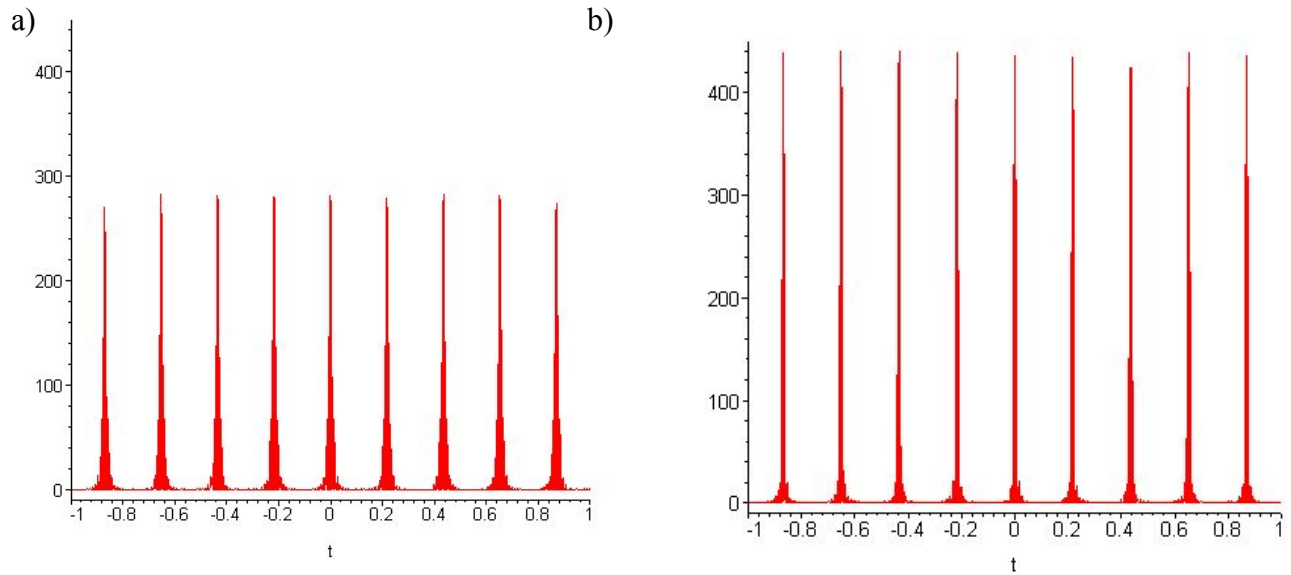


Fig. 4: Simplified Output of Multi-mode laser. Pulsed output based on twenty oscillating frequencies or modes, with a phase relation ϕ_j between the modes. **a)** Square phase $\phi_j = \phi_0 j^2$ relation between 20 oscillating modes. **b)** Phases all equal $\phi_j = \phi_0$. One can clearly observe that mode-locking produces the shortest pulses, with the FWHM changing by about a factor of $\frac{1}{2}$.

2.3 Mode-Locking Methods

There are two general methods for generating mode-locked laser output: passive mode-locking, commonly used with high power laser sources, and active mode-locking, implemented in this research.

Passive mode locking is based on the presence of a saturable absorber in the laser cavity. The saturable absorber will only reflect laser light with an intensity above a threshold, absorbing

all incident light below that threshold. Laser pulses with a higher intensity are thus selectively amplified, a process favoring mode-locking and high bandwidth pulses since they offer the shortest and highest intensity pulses [4]. The high intensities required for passive mode-locking are generally produced with Titanium Sapphire lasers or fiber ring lasers, greatly increasing the expense of the system. Also, saturable absorbers are sensitive to the frequency of the light and a specific knowledge of the laser cavity is therefore required. While offering femto second pulses and a massive comb width (on the order of 100 THz), a passive mode-locking system is very costly. If some comb width could be sacrificed, a significantly less expensive method, based on a diode laser, would be beneficial.

Our research makes use of active mode locking. Active mode locking is achieved through the addition of an external cavity to a normal diode laser and the periodic modulation of cavity losses. With many lasers, the gain medium has a limited bandwidth, and to perform active mode locking requires an additional acousto- or electro-optic modulator in the laser cavity; fortunately, diode lasers have a large gain bandwidth, allowing us to directly modulate the driving current for the gain medium. The mode-locking behavior occurs through the following process: the gain medium, in CW mode, is driven with a constant current, producing the central oscillating mode of the laser diode cavity ω_0 . An RF modulation at frequency ω_m is added to the constant driving current, causing sidebands at $\omega_q \pm \omega_m$. The external cavity added to the laser offers an infinite number of potential modes ω_q :

$$\omega_q = q2\pi \frac{c}{2L} = q2\pi FSR \quad (3)$$

where c is the speed of light, L is the length of the cavity, and FSR is the free spectral range¹, and q is an integer. While there may be infinite modes available, the number present in the cavity will be determined by the gain bandwidth of the diode laser. If the RF modulation of the gain medium is at an integer multiple or division of the cavity's free spectral range, the sidebands will fall on nearby cavity modes, amplifying each additional mode, producing a pulse in the cavity, as seen in Figure 2. In the time domain, when the diode driving current is modulated at resonance with the external cavity, the gain medium will be peaked when the pulse train arrives. The pulse wings nonetheless experience slight attenuation, gradually shortening the pulse with each round trip, and thus amplifying modes with a linear phase relation [4]. A schematic of the active mode-locking set-up is pictured in Figure 5.

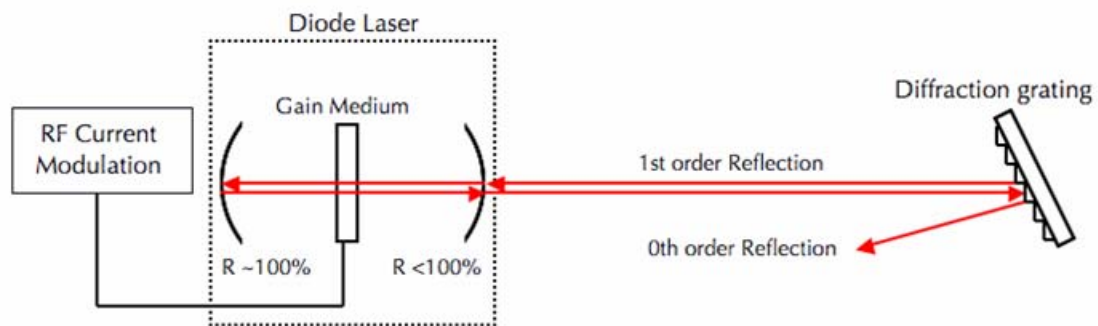


Fig. 5: Schematic diagram of active mode-locking diode laser An external cavity, defined by the diffraction grating, is added to a diode laser. The 0th order reflection from the grating exits the cavity and the 1st order reflections return to the laser. The driving current for the gain medium is modulated at the external cavity's FSR by an RF source.

3. Laser Apparatus

Our external cavity diode laser (ECDL) is implemented in a Littrow² configuration: the external cavity is defined by a diffraction grating (not an imperfect mirror as depicted in Fig. 5). The 0th order reflection becomes the output, and the 1st order reflection returns directly back to

¹ Free Spectral Range (FSR): Speed of Light over path length in cavity: $c/2L$

² See Parchotta [4], External-cavity Diode Lasers.

the diode. The set up is depicted in Fig. 6. We used a diode laser (Sanyo DL-7140-201W), with wavelength of 782 nm. Mounted on a Peltier thermoelectric cooler for temperature control, a collimating tube holds both the diode and collimating lens. We directly modulated the driving current of the diode laser gain medium with an RF signal.³ The RF signal was added to the constant driving current in a Bias Tee. The RF signal, originally at -7 dBm, is amplified by a 30 dB amplifier (not pictured), resulting in a signal of about 23 dBm. The signal enters the Bias Tee via a circulator, protecting the amplifier from potential reflections. The external cavity was built so that the FSR of the cavity would be between 400 MHz and 500 MHz, as prior research performed by DeSalvo indicated that such a cavity length worked best [5]. As shown in Figure 6, the diode and cavity were both mounted on a large optical breadboard to reduce independent vibrations of components.

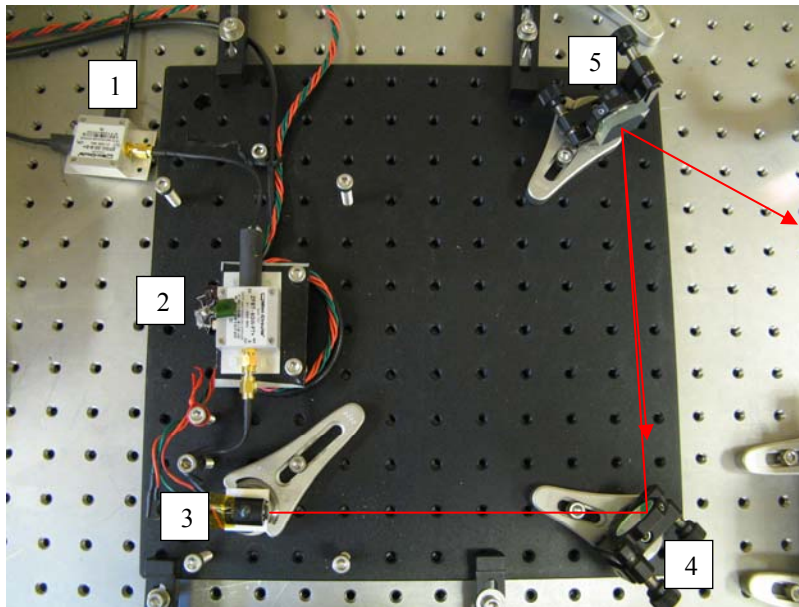


Fig. 6: Laser Diode and External Cavity A directional coupler (1), protects RF source; RF signal enters Bias Tee (2) which combines driving current with RF gain modulation; (3) laser in collimating tube mounted on a thermoelectric Peltier cooler; outputs to external cavity defined by mirror (4) and diffraction grating (5). The diffraction gradient reflects the 1st order reflection back into the diode laser and the 0th order out of the cavity, indicated by the arrows.

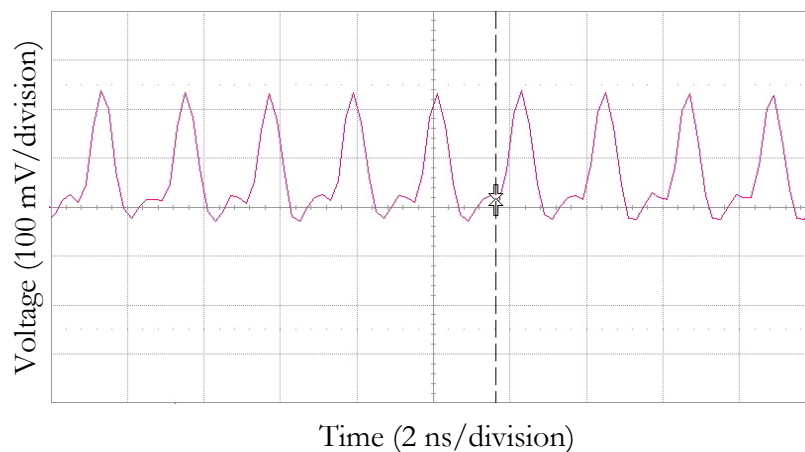
³ Our source can output a 13dBm sinewave over 100 KHz to 2.1GHz (HP 8657B RF source)

3.1 Laser Diode Operating Modes

The controlling unit of the laser⁴ provides two operating modes for the laser diode, constant current and scanning. The constant current mode is the normal operating mode, used for both CW and mode-locking outputs. The scanning mode is used for cavity alignment. When properly aligned, the external cavity will lower the lasing threshold driving current. By scanning around an offset voltage and observing the output of the laser, we are able to align the cavity. Preliminary characterization of the diode gave us an initial threshold value for the laser of 35.6 mA \pm 1 mA. After alignment, the threshold dropped to 30.45 mA \pm .74 mA, a notable 15% decrease in threshold current with the addition of the cavity.

3.2 Preliminary Pulse Analysis with Fast Photodiode

Preliminary characterization of the external cavity was then performed using a fiber input Silicon fast photodetector with a 1.2 GHz bandwidth (ThorLabs DET02AFC). Fig. 7 clearly demonstrates a pulsed output from the laser system.



⁴ For more information on the laser control unit, see Desalvo, 2008 [5].

Fig. 7: Nanosecond Pulses, as measured by Fast Photodiode Full width at half max of the detected pulses is approximately 1 ns, but limited by the bandwidth of the detector. The small secondary pulses weren't fully understood, but the diode producing this particular pulse train broke. The current diode produced a similar image, but without secondary pulses. RF modulation of the laser gain medium is at 460 MHz.

Direct measurement of the pulse width seems to be constrained by the 1.2 GHz bandwidth of the fast photodiode and the 1 GHz bandwidth of the oscilloscope. We scanned through the RF frequency modulations from 200 MHz to 550 MHz at intervals of 10 MHz to find the free spectral range (FSR) of the external cavity. The results are pictured in Figure 8, with a clear resonance at 230 MHz and 460 MHz, and non-resonance at 345 MHz. As such, 460 MHz was determined to be the cavity's FSR.

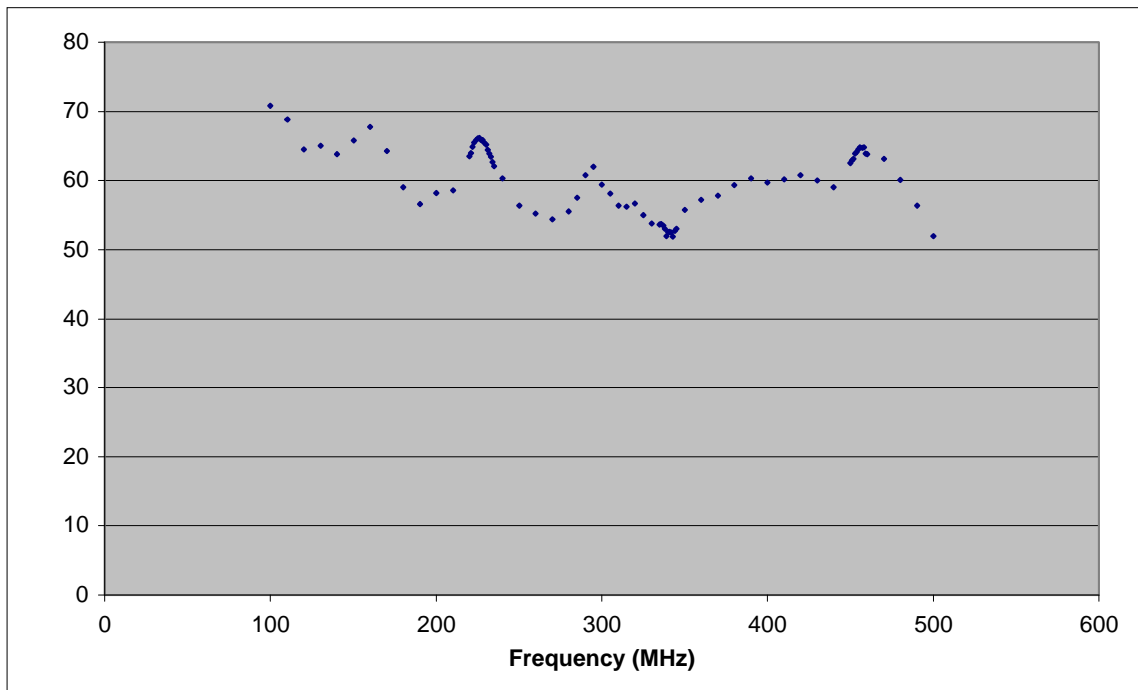


Figure 8: Frequency vs. Pulse Magnitude (RMS) Scanning across 100 MHz – 500 MHz, characterized the pulsed output. The largest magnitudes arise at multiples of the cavity FSR – found to be 460 MHz. Smallest magnitude found at half-integer multiple of FSR.

While determining the amplitude of the pulses to find resonances, the pulse FWHM was also recorded, with the results depicted in Fig. 9. Prior to about 300 MHz, the pulses are not limited by detection methods, and seem to progress linearly down. At about 300-350 MHz, we

observe the limits of detection methods. The cavity FSR was found to be 460 MHz. Extrapolating the trend down to the cavity FSR, we expected pulses somewhere between 600 to 200 ps. Observing the behavior at 230 MHz modulation (half the resonance value) indicates that the extrapolations may be a conservative estimate: the pulse width drops dramatically from values associated with neighboring frequencies. If similar behavior occurs at 460 MHz, the pulses may be significantly smaller than 200 ps.

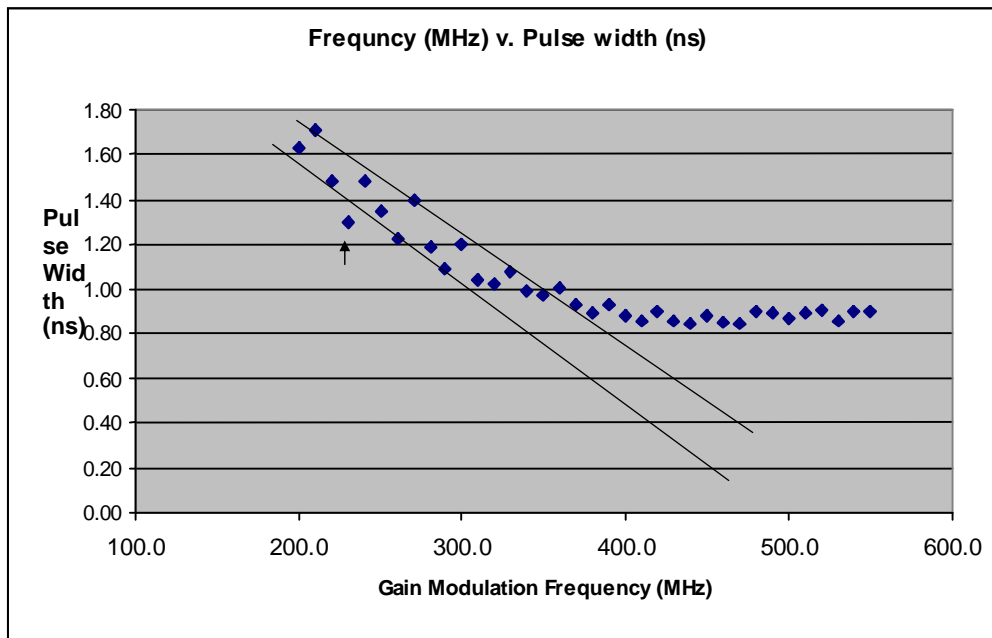


Figure 9: Gain Modulation Frequency v. Pulse Temporal Full-Width At 300 MHz, the 1ns limit of the detector becomes evident. The two black lines display the range of extrapolations down from the non-limited section to the cavity resonance frequency of 460 MHz. Also, note the decrease in pulse width from neighboring values at 230 MHz, half the resonant value (indicated by the arrow). This behavior indicates improvements in performance at cavity resonances associated with active mode-locking.

4 Sub-Nanosecond Pulse Detection Methods

With hints of sub-nanosecond performance, a new method of characterization was required. Two methods were implemented: a scanning Fabry-Perot cavity, with which one can directly measure comb width; and a Michelson interferometer in an autocorrelator configuration, with which one can indirectly measure pulse width.

4.1 Fabry-Perot

A Fabry-Perot cavity is composed of two highly reflective mirrors which transmit light only when the optical path length of the cavity is an integer multiple of half the wavelength of the incident light beam. In a scanning Fabry-Perot cavity, one of the mirrors is translatable, mounted on Piezo electric transducer. By modulating the cavity's FSR, the scanning Fabry-Perot essentially performs a Fourier transform on the incident light beam, transmitting the various frequencies composing the input light as a function of cavity length. The breadth of the frequency comb associated with picosecond length pulses makes commercially available scanning Fabry-Perot cavities insufficient, and so a custom scanning Fabry-Perot was built in the lab, as pictured in Figure 10. Details of the construction can be found in DeSalvo 2008 [5].



Figure 10: Custom Fabry-Perot The lens (far left) focuses the beam into the Fabry-Perot cavity. The cavity mirrors are planar and both fully adjustable on x- and y-axes. The second mirror was driven by Piezo electric transducer, creating the scanning cavity.

This method should be able to directly measure the breadth of the comb and the width of the pulses could therefore be inferred from the transform equation. Unfortunately, the custom built Fabry-Perot interferometer was unsuccessful in measuring the comb width due to the broad linewidth of the cavity, though it may still be useful with more meticulous alignment and better mirrors.

4.2 Michelson Interferometer as Autocorrelator

The Michelson interferometer as autocorrelator is the most common way to measure pulses in the picosecond and femtosecond range. The interferometer uses high accuracy spatial resolution to improve temporal resolution. The Michelson interferometer is composed of a 50/50 beam splitter that divides the input, directing it to two mirrors, one stationary and one translatable. The two beams are then recombined, generating an interference pattern. At this point, direct detection offers a first-order autocorrelation, or an electric-field autocorrelation.

Unfortunately, the first order autocorrelation function only provides information on the coherence length and bandwidth of the comb, and does not offer any direct information on the pulses themselves. Pulse width information requires a second order autocorrelation, or intensity-intensity autocorrelation. To perform this in-lab requires a non-linear element. As depicted in Figure 11, the non-linear crystal doubles the frequency. To then detect the intensity autocorrelation, one must filter out the original frequency, and use sensitive detection methods, such as a Photomultiplier tube, to observe the doubled frequency.

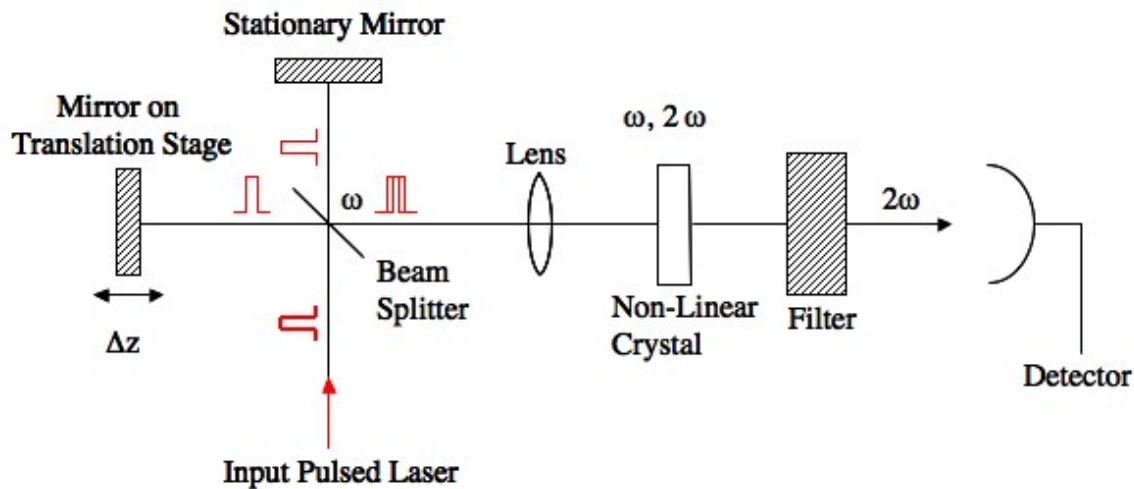


Figure 11: Michelson Interferometer as Autocorrelator The input pulse is divided at the beam splitter, going to a stationary and a translatable mirror. Recombining at the beam splitter, the pulses will now be offset proportional to the difference in the path length Δz , producing an interference pattern. For pulse information, a second-order autocorrelation is required: the lens focuses the combined red pulses onto a non-linear crystal, doubling the frequency, producing blue light. The filter removes the red light and the blue light enters a PMT for analysis. Figure adapted from Demtroder [6].

4.2.1 First Order Autocorrelation - Theory

The first order autocorrelation is an indicator of the temporal coherence of light [3]. The first order auto correlation function is defined by the following equation:

$$g^{(1)}(\tau) = \frac{\langle E^*(t)E(t+\tau) \rangle}{\langle |E(t)|^2 \rangle} \quad (4)$$

where the $\langle \rangle$ symbol indicates a time average over a long interval T , and τ is the temporal difference between the pulses due to the difference in path length. Assuming an electric field centered around ω_0 , with some broadband variance $\phi(t)$:

$$E(t) = E_0 e^{-i\omega_0 t} e^{i\phi(t)} \quad (5)$$

Substituting this into Equation 3, the first order autocorrelation becomes:

$$g^{(1)}(\tau) = e^{-i\omega_0 \tau} \langle e^{i[\phi(t+\tau) - \phi(t)]} \rangle \quad (6)$$

The first part of the expression is then a rapid oscillation with produces the fringe pattern observed in interference experiments, while the second part contains the information on the light's coherence. In an interference experiment, the fringe visibility is directly related to the real part of the first-order autocorrelation [3]:

$$|g^{(1)}(\tau)| = \text{visibility} = \frac{I_{\max} - I_{\min}}{I_{\max} + I_{\min}} \quad (7)$$

Unfortunately, the visibility does not contain any information on the pulse's time profile if the detector's time constant $T \gg \tau$, which is always the case [6].

4.2.2 Second Order Autocorrelation

The second order autocorrelation is an intensity autocorrelation. It can be expressed with by the following equation [3]:

$$g^{(2)}(\tau) = \frac{\langle E^*(t)E^*(t+\tau)E(t+\tau)E(t) \rangle}{\langle E^*(t)E(t) \rangle \langle E^*(t+\tau)E(t+\tau) \rangle} = \frac{\langle I^*(t)I(t+\tau) \rangle}{\langle I(t) \rangle \langle I(t+\tau) \rangle} \quad (8)$$

In practice, to perform an intensity-intensity autocorrelation requires a non-linear element. By focusing the two pulses into a frequency doubling non-linear optical element, the intensity of the generated second harmonics is proportional to the square of the incident intensity:

$$I(2\omega) \propto (I_1 + I_2)^2.$$

The expected signal for the second order autocorrelation is thus:

$$\begin{aligned} \langle \text{Signal}(2\omega, \tau) \rangle &= \frac{a}{T} \int_{-T/2}^{+T/2} I(2\omega, t, \tau) dt \\ &= a \left[\langle I_1^2 \rangle + \langle I_2^2 \rangle + 2 \langle I_1(t)I_2(t+\tau) \rangle \right] \end{aligned} \quad (9)$$

While the first two terms in this expression are independent of τ and provide only a constant background, the third term depends on the delay time τ and offers information on the pulse profile $I(t)$ [6].

There are two ways to experimentally implement the second order autocorrelation. The first is the method depicted in Figure 11, with both beams following the same path to the non-linear crystal. Because this setup allows through the background signal $\langle I_1^2 \rangle$ and $\langle I_2^2 \rangle$ in Equation 8, one must account for this in data analysis. A more robust way to perform this autocorrelation is a noncollinear correlation. In this set-up, the two beams are focused on the non-linear crystal from two different angles. Only when energy and momentum conservation are satisfied will a

blue photon emerge in the proper direction. As this occurs only when a photon from each beam overlaps, the resultant signal is composed entirely of the non-linear component⁵.

5. Detection of Picosecond Pulses

5.1 Experimental Implementation of Michelson Interferometer as Autocorrelator

The experimental setup, following the schematic in Figure 11, is pictured in its experimental setup in Figure 12. For femtosecond lasers, the translatable mirror would typically be attached to an audio speaker. For the picosecond laser pulses predicted from preliminary results, our research required greater translation magnitudes. From Table 1, it is evident that if our pulses are as long as 600 ps, this will require a translation of 9.0 cm. The initial set-up allowed for the 9 cm requirement by placing a micrometer translation stage on an optical breadboard. From qualitative analysis, it was quickly recognized that the pulses were significantly shorter, requiring only the 12 mm micrometer translation stage for analysis.

$\Delta\tau$	600 ps	200 ps	100 ps	50 ps	10 ps	5 ps	2 ps	1 ps
Δx	9.0 cm	3.0 cm	1.5 cm	7.5 mm	1.5 mm	.75 mm	.30 mm	.15 mm

Table 1: Translation Stage Changes Δx for Temporal Overlap $\Delta\tau$ of Pulses Values are based on the relation $\Delta\tau = 2(\Delta x/c)$, where $\Delta\tau$ is the overlap, Δx is the spatial change of the translation stage, and c is the speed of light. The factor of two arises from the fact that the light travels the interferometer arm twice. Resolution of the micrometer translation stage is .01 mm.

⁵ For more information on Noncollinear Intensity Correlation, see W. Demtroder p. 653 [6]

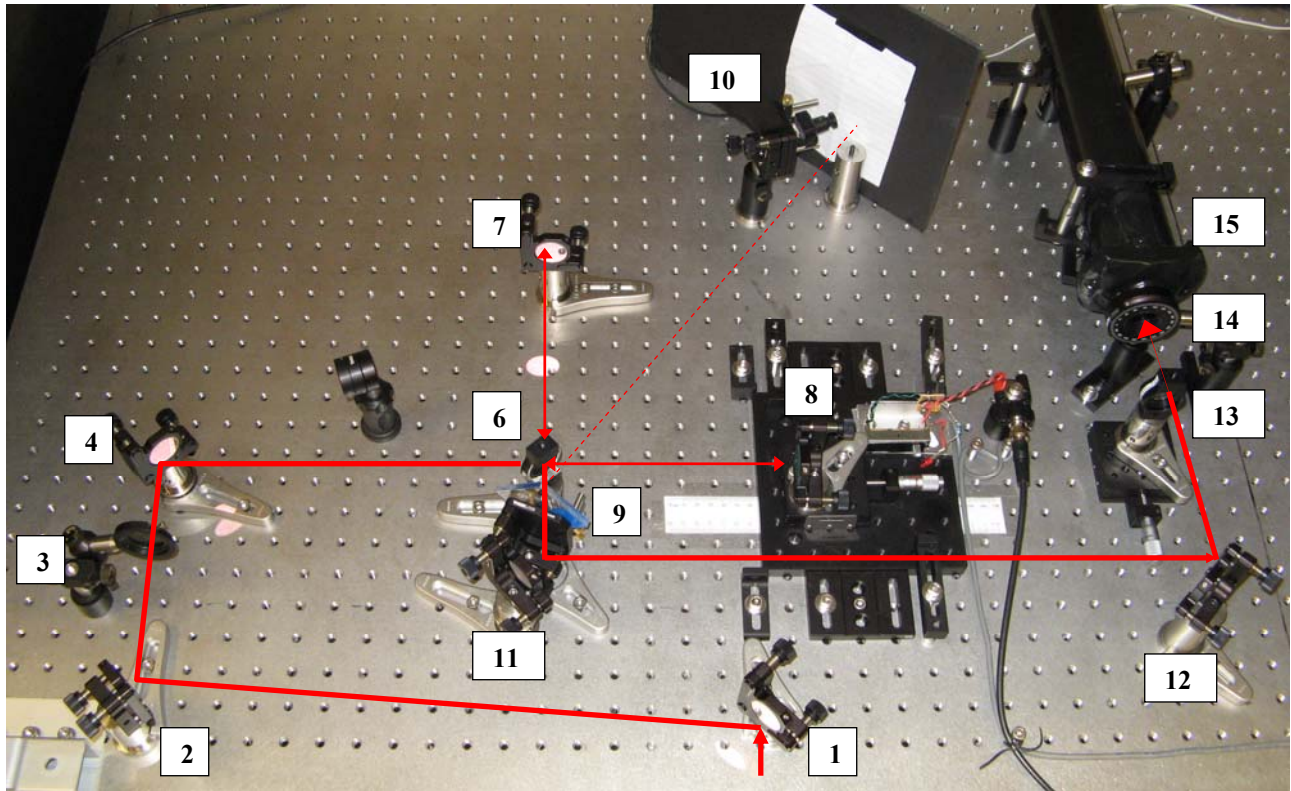


Fig. 12: Experimental Setup of Michelson Interferometer as Autocorrelator Laser light enters set-up at mirror (1) and is raised from the plane of the table via mirrors (1,2,4). Iris (3) adjusts beam shape. The beam is divided at 50/50 beam splitter (6), traveling to a stationary mirror (7) and a mirror on a translation stage (8), returning along the same path to the beam splitter (6). The glass plate (9) deflects a tiny bit of the output (2%-4%) to the CCD camera (10), allowing direct observation of fringes for alignment and quick qualitative analysis. The interferometer output is directed, via mirrors (11,12) into a lens (13). The light is focused to a point on the non-linear crystal (14), doubling the frequency of the light, and then enters the detector, a photon counting PMT (15).

5.1.1 First-Order Autocorrelation with Michelson Interferometer

The initial first order auto-correlation results are depicted in Figure 13. The data was collected prior to the addition of the non-linear crystal, filter, and PMT to the set-up, with the lens focused on a normal photodiode. Also, the translation stage (Element 8 in Figure 12) is pictured with an automated position measurement apparatus. The apparatus was added after first-order data collection. Each data point in Figure 13 was taken manually.

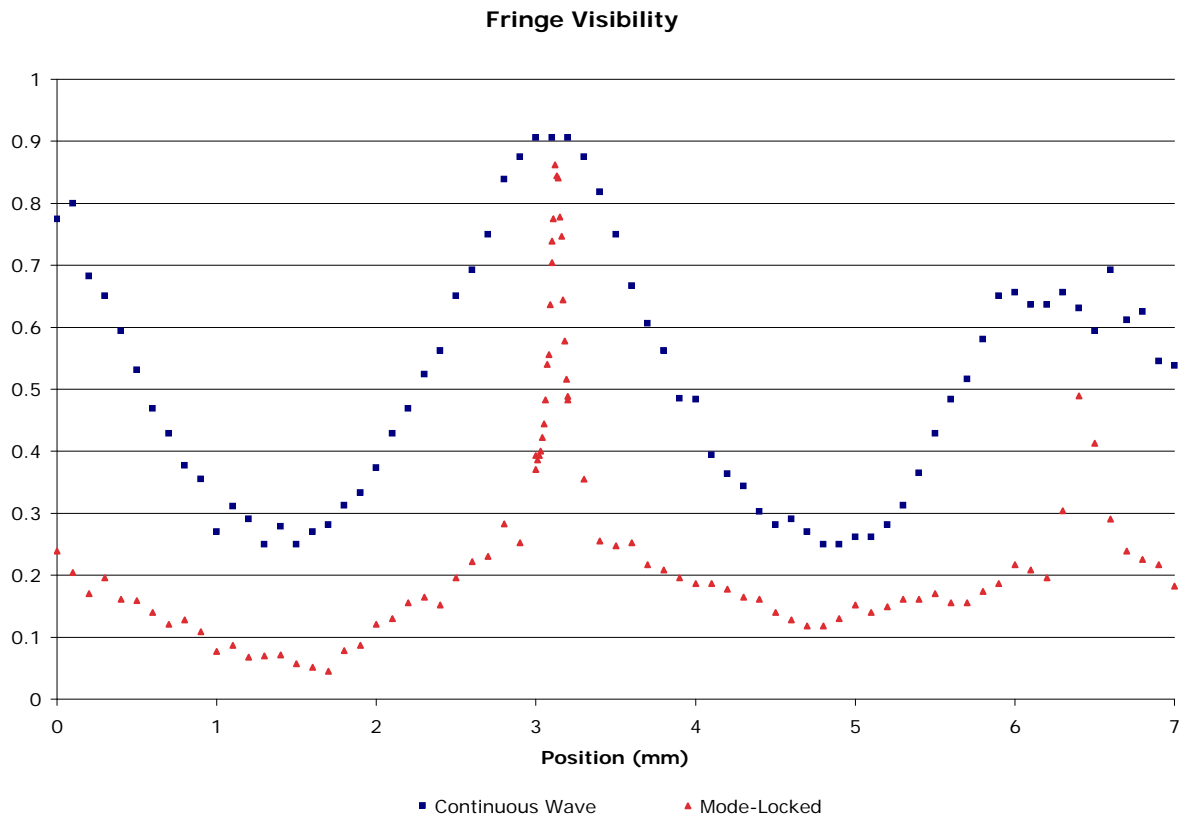


Figure 13: Fringe Visibility The red triangles indicate the fringe visibility of the mode-locked laser. The blue circles depict fringes with the laser outputting continuous wave. The peak FWHM for the mode-locking signal is .15 mm, which translated to temporal scale, is about 1 ps. When outputting a continuous wave (CW), the laser shows hints of self mode-locking as well, with a FWHM of 15 ps.

A definite peak in fringe visibility occurs for the mode-locked signal when the path lengths are equal. The full-width at half-max (FWHM) is .15 mm, which translated into a temporal width is on the order of 1 ps. While not yet a measure of pulse width, the feature indicates a coherence time on the order of 1 ps. Such coherence time will only occur for a broadband output and therefore provides solid evidence of a spectral comb width on the order of 300 MHz. Another interesting feature in Figure 13 is the secondary peak at 6.4 mm. Though not investigated as thoroughly, this may be due to a secondary cavity created with the diffraction grating and the diode window. Also of interest is the continuous wave (CW) laser displaying changes in fringe visibility, hypothesized to be self mode-locking of the diode laser due to the external cavity.

However, since no pulses were observed with the fast photodiode without RF modulation of the gain medium, the behavior may simply be a coherence time effect. Also, the shape of the mode-locking signal from 2 mm to 5 mm – a low hill from which the narrow peak arises – may be a superposition of self locking and active mode locking effects. Further investigation, in the form of a second order autocorrelation, should help to determine if the laser is self mode-locking without gain modulation. A re-centering of the translation stage will also allow investigation of a potential secondary pulse symmetric to the one at 6.4 mm.

5.1.2 Second Order Autocorrelation with Michelson Interferometer

Since the second order autocorrelation required a non-linear element, either in the form of a non-linear optical element, or a detector with a non-linear response. Some preliminary investigation into two-photon absorption in photodiodes and LEDs was performed. Although Sharma, *et al.* [7] detected picosecond pulses using two photon absorption in AlGaAs LEDs, concern that our laser power was not powerful enough put the research on hold. Instead, the more traditional method of a non-linear crystal with a photo multiplier tube (PMT) in photon counting mode was selected. The non-linear crystal is a Beta-Barium Borate crystal from the laboratory of Professor Jan Chaloupka. Being sensitive to polarization, it was mounted in a rotation stage. A 400 nm band pass filter protected the PMT from extraneous red photons, blocking roughly half the blue photons as well. Also, the PMT has a peak response at around 400nm, dramatically attenuating light at 780 nm⁶. The PMT signal required supporting electronics: pulse signal went to an amplifier, then to a discriminator (which reduces ‘dark’ photons – those produced by random thermal activity inside the PMT). From the discriminator,

⁶ Attenuation factor better than 10^2 but unknown: 780 nm beyond range of values in PMT characterization

the signal goes to a pulse counter, which outputs a voltage proportional to the number of pulses the counter receives.

With the non-linear crystal in place, everything aligned, and the laser mode-locking, and a strong signal from the PMT, the setup was tested for non-linear behavior. Attenuating the input signal to the Michelson interferometer with various neutral density filters, we observed the signal response at the PMT. The results are depicted in Figure 14 and provide distinct evidence of second harmonic generation, or blue light, since the signal is quadratic in intensity.

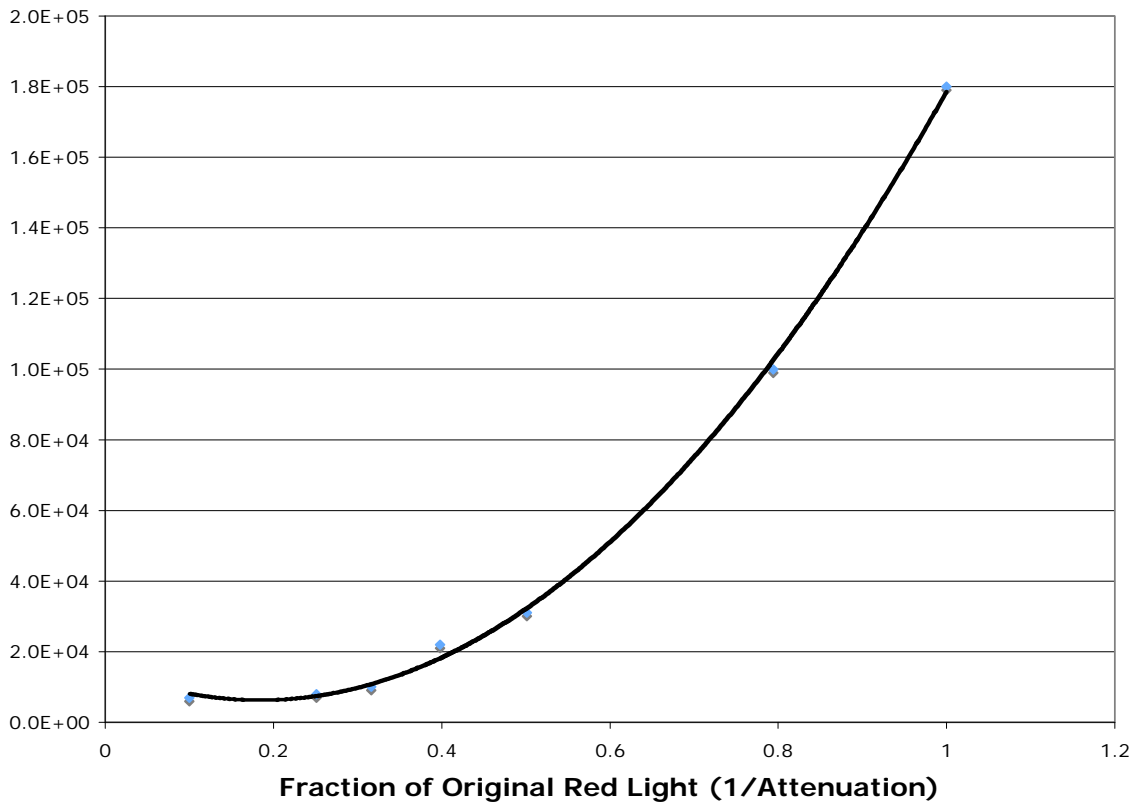


Figure 14: Blue Light vs. Red Light Attenuation The number of photons counted at the PMT as a function of 1/Attenuation Factor. The trendline, a 2nd-degree polynomial, clearly indicates non-linear response to attenuations: second harmonic generation is definitely occurring. Error bars are present for possible error in attenuation factor labeled for each neutral density filter. More comprehensive error analysis was not performed as the goal was only to determine with confidence the existence of a non-linear effect.

To accelerate the speed of data collection for second order autocorrelations, an apparatus automating the measurement of translation stage position was built. Attaching the arm of a linear slide potentiometer to the side of the translation stage, an adjustment in position adjusted the resistance of the potentiometer. The output voltage, directly proportional to the position, was collected by the scope. Upon calibration, the resolution was found to be $\pm 0.03\text{mm}$, but unfortunately when implemented, the oscilloscope offered only 0.2 mm position increments. To reclaim some resolution, the data was processed with a running average: every 5 raw data points were averaged to generate each point in the following results.

The results of the second-order autocorrelation are depicted in Figures 15 and 16. There is clear pulse behavior from about 5.25 mm to 5.50 mm. The translation stage was mounted so that the interferometer arm lengths were approximately equal at the position $5.3\text{ mm} \pm 0.1\text{ mm}$ on the translation stage. In both figures, the pulse width is on the order, temporally, of $1.5\text{ ps} \pm .03\text{ ps}$. Fig. 15 also indicates additional pulse train behavior to the left of the central pulse. However, second-order correlations do not show physical asymmetries in the pulse train, therefore the asymmetry present is most likely due to a slight angular deviation between the translation axis and the axis of the interferometer arm. In Fig. 15, the peak intensity of the pulse signal is about 10 V, which is actually the max output of the rate meter. A neutral density filter, with attenuation of about a factor of 2, was placed prior to entry into the interferometer to prevent this, giving Fig. 16. There, the pulse train is attenuated but the maximum intensity – where the pulses are presumably overlapping – is dramatically more than non-interfering areas. This indicates that the rate meter was saturated in Figure 15.

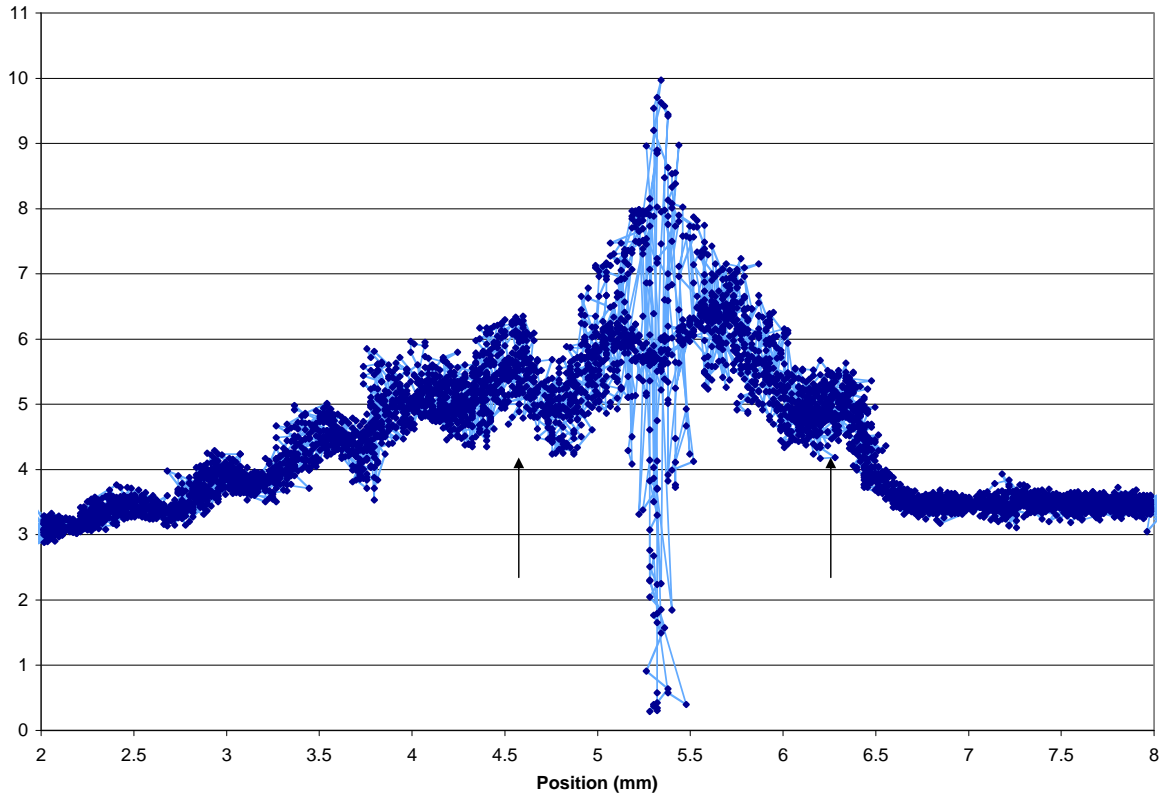


Fig. 15: Second Order Autocorrelation Each data point average of 5 collected points. The x-axis indicates the position of the translation stage. The stage was centered so that the position $x = 5.3$ was the point at which the two interferometer arm lengths were equal. We observe clear pulse behavior from 5.25 mm to 5.50 mm. The FWHM is $0.25 \text{ mm} \pm .05 \text{ mm}$ – a temporal width of $1.7 \text{ ps} \pm 0.3 \text{ ps}$. Secondary pulse shapes, on the left side of the central pulse, indicates the presence of smaller secondary pulses. The arrows indicate symmetric secondary pulses. The fall off on the right side suggest possible misalignment of the translation stage. The rate meter has a maximum output of 10 V, so central pulse signal may be larger than pictured.

The arrows in Fig. 15 indicate two sideband pulses, suggesting that similar secondary pulses observed in the first-order autocorrelation are indeed part of the actual pulse train. As mentioned previously, second-order autocorrelations do not reveal any asymmetry in the pulse train, so if such knowledge becomes significant, a third-order autocorrelation may be necessary.⁷ The side pulses are offset from the central pulse by about 1.5 mm spatially (10 ps temporally) which translates to a frequency difference of about 200 GHz between central and secondary pulses. If the secondary pulses are created due to an extra cavity in the laser system, by the

⁷ See FROG Technique, Demtroder, p. 657 [5].

relation $FSR = c/2L$, the frequency difference of 200 GHz would be generated by a cavity difference of approximately 1.5 mm. This measure is on the scale of the laser diode, and since there is no anti-reflective coating on the protective window of the laser diode, we hypothesize that this is the cause of the secondary pulses.

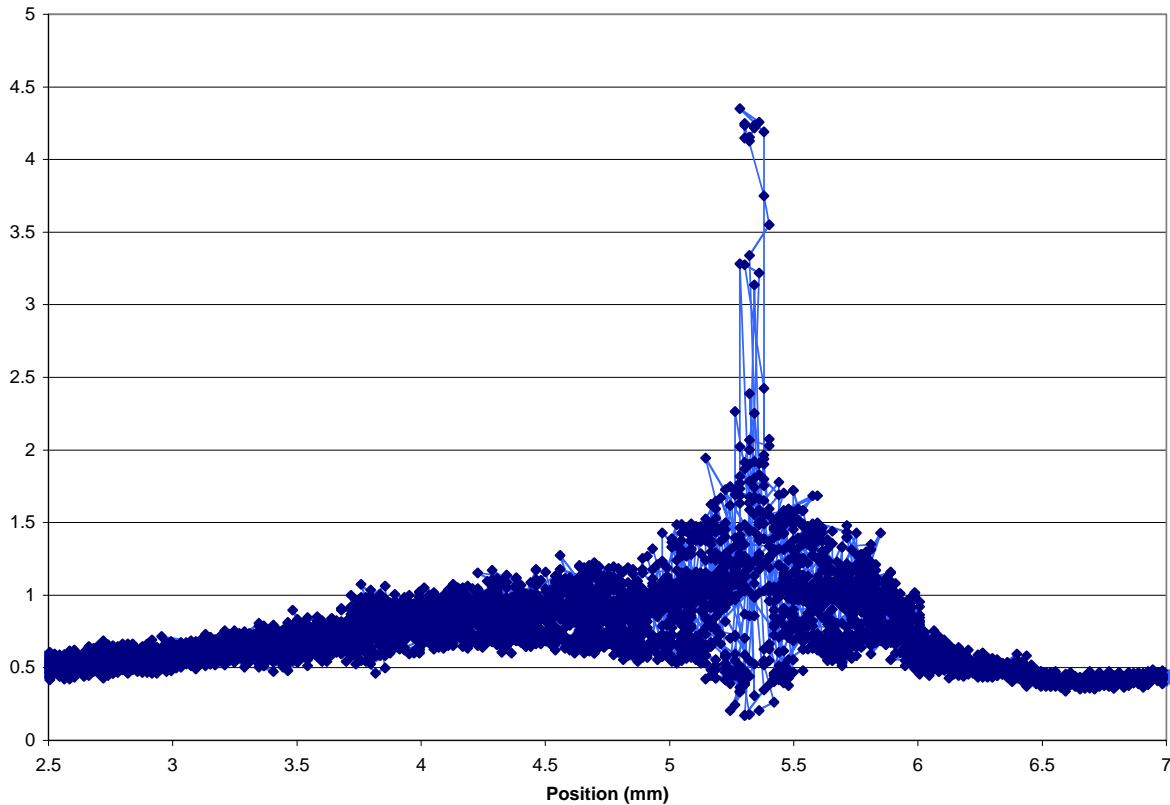


Fig. 16: Second Order Autocorrelation – Attenuated Light A neutral density filter, attenuation factor 10^3 , kept the rate meter from saturating. Each data point is the average of 5 measured values. Similar behavior to Figure 15 observed, with the pulse FWHM $.2 \text{ mm} \pm .05 \text{ mm}$. This is a *temporal width of $1.4 \text{ ps} \pm 0.3 \text{ ps}$* . The signal drop off occurs once again at 6 mm, possibly due to translation stage alignment inaccuracy.

Since position-dependent fringes were observed for the laser outputting without RF modulation of the gain medium, we turned off the RF modulation and performed a second order autocorrelation on the “continuous wave” laser output. The results, displayed in Figure 17, offer

strong evidence of self mode-locking behavior. The FWHM is approximately $10 \text{ ps} \pm 2 \text{ ps}$, and the secondary pulses, though slightly more obscure, are still evident.

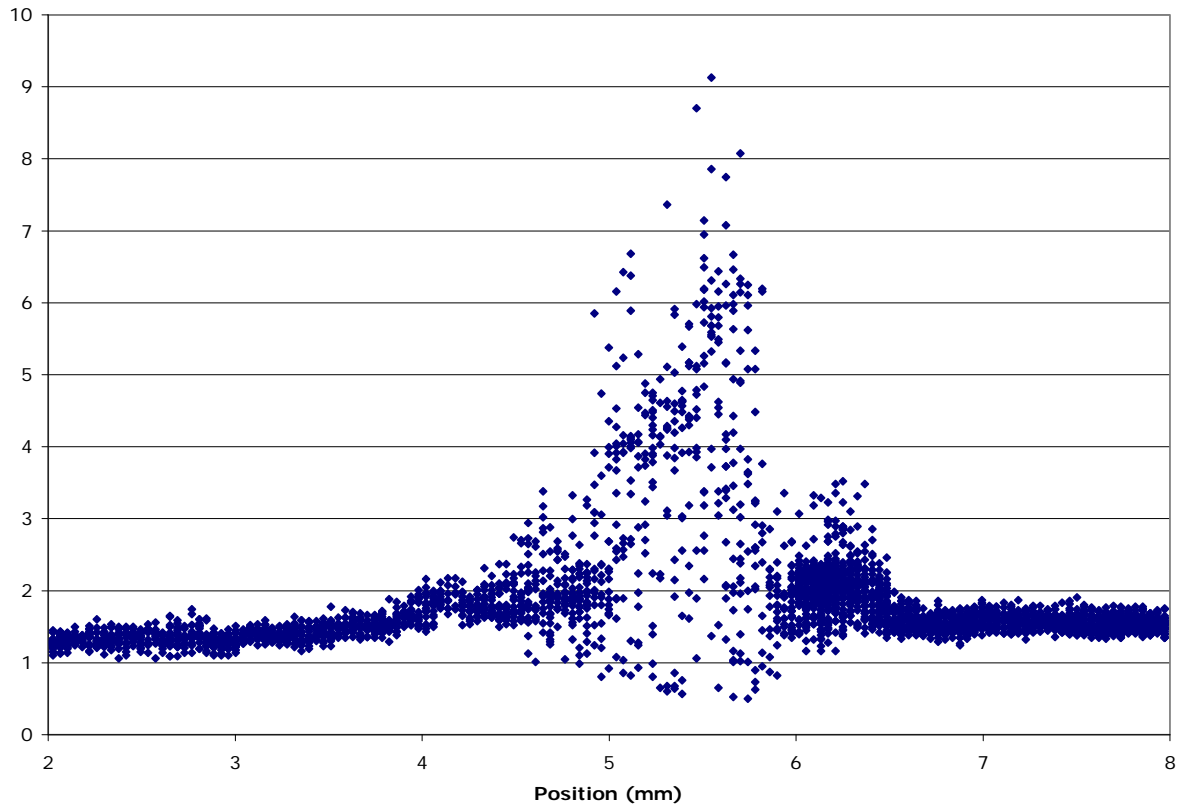


Fig. 17: Second Order Autocorrelation for “Continuous Wave” Laser Output There is no RF modulation of the gain medium inducing active mode-locking. The autocorrelation indicates that the laser with external cavity is self mode-locking. The FWHM is about 10 ps. Each data point is the average of 5 measured values, though here, the limits of oscilloscope resolution are apparent in the discrete position values.

5.1 Conclusion

Pulses have successfully been generated using an actively mode-locked diode laser with external cavity. Indirect measurement of these pulses was performed using a Michelson interferometer as an autocorrelator. From first order (electric field-electric field) autocorrelation, it can be confidently concluded that the multi-mode output of the laser has a bandwidth of at

least 300 GHz and possibly as large as 1 THz. This should be adequate for the example case given in the introduction demanding stabilization of a laser at the francium trapping wavelength with a nearby Neon I transition, though better analysis of comb and pulse width will be required prior to implementation. Direct observation of the frequency comb with a custom built scanning Fabry-Perot cavity was unfortunately unsuccessful. Using a second order (intensity-intensity) autocorrelation, pulses on the order of 1.5 ps have been measured. Also, passive pulse generation (no RF modulation of the laser gain medium) has been observed.

Currently, second order autocorrelation measurements may be suffering from an angular deviation between the translation stage and interferometer arm. Accuracy of autocorrelation measurements could be improved by removing this angular deviation. With strong evidence of pulses on the order of 1.5 ps, however, indicates a translation distance of only 2 mm should be required, which may enable the implementation of an audio speaker as a translation stage. Such improvements will precipitate faster data acquisition and analysis, which will be necessary before optimization of temporal pulse width and spectral comb width can be performed. While the comb width may currently be satisfactory, optimizing pulse width, and therefore increasing peak intensity, may allow the implementation of a saturable absorber, creating a hybrid mode-locking system. Also, further numerical modeling, such as can be performed in MAPLE, of lasing modes inside the cavity may aid in understanding the passive self mode-locking observed, as well as pulse train shape. Improvements in scanning Fabry-Perot alignment, as well as possibly changing out planar mirrors for spherical mirrors, could allow direct observation of the comb. With these various developments, the actively mode locked laser diode with external cavity may then be implemented for optical frequency measurement and stabilization in an Ultra-cold Atomic, Molecular and Optical physics laboratory.

References:

- [1] S.T. Cundiff and L. Hollberg. Absolute Optical Frequency Metrology in Encyclopedia of Modern Optics B.D. Guenther and D.G. Steel, eds, (Academic Press, 2004).
- [2] J. Ye, H. Schnatz and L.W. Hollberg Optical frequency combs: from precision frequency metrology to optical phase control. IEEE J. Selected Topics Quantum Electronics 9, 1041 (2003).
- [3] M. Fox. Quantum Optics: An Introduction. Oxford University Press, New York 2006. p. 17-19, 211.
- [4] R. Paschotta. Encyclopedia of Laser Physics and Technology. Wiley 2008. Electronic Version.
- [5] B. DeSalvo. "Mode-Locked Diode Laser for Precision Optical Frequency Measurements." Undergraduate Thesis. College of William and Mary. (2008)
- [6] W. Demtröder. [*Department of Physics, University of Kaiserslautern*] *Laser Spectroscopy*. 3rd ed. (Springer Verlag, Berlin, 2003). p. 648-53.
- [7] A.K. Sharma, *et al.* "Use of commercial grade light emitting diode in auto-correlation measurements of femtosecond and picosecond pulses at 1054 nm" Optics Communications 246 (2004) p 195-204.

Appendix A: Standard Operating Procedure

A.1 Turning laser on:

1. **Ground yourself**
2. Check to ensure coupler not connect to laser. If so, disconnect it.
3. Turn amplifier power on (28.0 V)
4. Turn RF source power on.
5. Turn RF source output signal off.
6. Plug coupler back into the laser.
7. Power on the laser. Allow temperature controller to stabilize.
8. Current switch to “on” position. Bring laser to operating voltage.
9. Safe to turn RF source output signal on as needed.

A.2 Turning laser off:

1. **Ground yourself**
2. Turn RF source output signal off (not the whole source, just the output)
3. Lower the laser output current until off.
4. Current switch to “off” position.
5. Turn laser power off.
6. Unplug coupler from laser.
7. Turn RF source off.
8. Turn amplifier power off.

A.3 Use of scanning mode:

1. Bring the laser to an operating level a bit above the threshold.
2. Attach function generator to Scan BNC connector.
3. Turn the current switch off and the scan switch on.
4. The inputted signal from the function generator changes the output voltage according the following equation:

$$I_{mod} = I_{op} - V_{mod} \frac{200mA}{5V}$$

I_{mod} is the modulated current delivered to the laser diode in milliamps

I_{op} is the operating current (set by the user in milliAmps)

V_{mod} is the voltage from the function generator, in Volts.

5. When in scanning, the user must be careful to keep I_{mod} positive, as negative values will break the laser diode. Good values are as follows:

$V_{monitor} = .586 \text{ V (45mA)}$

Function generator: Triangle wave, 512 mV pk-pk, +265 mV offset.

This scans 25 mA to 45 mA, around threshold 35 mA.